LA-UR-14-21257

Approved for public release; distribution is unlimited.

Title: Calibrating the Abaqus Crushable Foam Material Model using UNM Data

Author(s): Schembri, Philip E.
Lewis, Matthew W.

Intended for: Report

Issued: 2014-02-27

Calibrating the Abaqus Crushable Foam Material Model using UNM Data

Philip Schembri and Matt Lewis, W-13

November 4, 2013

Summary

Triaxial test data from the University of New Mexico and uniaxial test data from W-14 is used to calibrate the Abaqus crushable foam material model to represent the syntactic foam comprised of APO-BMI matrix and carbon microballoons used in the W76. The material model is an elasto-plasticity model in which the yield strength depends on pressure. Both the elastic properties and the yield stress are estimated by fitting a line to the elastic region of each test response. The model parameters are fit to the data (in a non-rigorous way) to provide both a conservative and not-conservative material model. The model is verified to perform as intended by comparing the values of pressure and shear stress at yield, as well as the shear and volumetric stress-strain response, to the test data.

1 Introduction

APO-BMI, also called syntactic foam, is a material used in LANL structural supports. APO-BMI is a bismaleimide (BMI) monomer cured using a reaction with the diamine agent Apocure-601 (APO). It forms the matrix of a syntactic foam around either glass (in the W88) or carbon (in the W76) microballoons. These syntactic foams are relatively rigid, brittle in tension, and crush repeatably at high enough compressive stress. APO-BMI replaced Kerimid 601 as the binder in these materials since Kerimid was found to be a carcinogen.

In 2004 a crushable foam material model of APO-BMI with carbon microballoons was calibrated by Matt Lewis(Lewis, 2004) for use in DYNA simulations (Material #5) using triaxial compression data from tests performed at the University of New Mexico (UNM)(Reser, Ahuja, & Lenke, 2004). A model of the same material, calibrated to the same data along with some recent data obtained by W-14(Kingston, 2013), is now calibrated for use in Abaqus. This report documents the calibration of the Abaqus Crushable Foam material model using the available test data. The report is arranged as follows: the material model is briefly described, the UNM and W-14 tests are summarized, the methods by which the test data is regressed and by which the material model parameters are obtained from the regressed data are described, and verification of the material model is presented.

2 Abaqus Crushable Foam Model

The Abaqus Crushable Foam material model is described in detail in Section 19.3.5 of the Abaqus Analysis Users Manual(Dassault Systèmes Simulia Corp, 2009); a summary, taken almost entirely from that reference, is provided here for completeness.

When loaded, a Crushable Foam material behaves linear-elastically up until a yield stress is reached. As such, Young's modulus and Poisson's ratio must be supplied to Abaqus through the *Elastic keyword. The initial yield stress in the Crushable Foam model is a function of pressure (i.e. the negative of the hydrostatic, or mean, stress). This pressure dependence is defined through a yield surface that is circular in the deviatoric stress plane and elliptical in the meridional stress plane (the plane parallel to both the Mises stress (q) and pressure (p) axes), as shown in Figure 1. Note that this differs from the most commonly used (e.g. for metals) yield surface, which is circular in the deviatoric plane but which is a line parallel to the pressure axis in the meridional plane (i.e, constant with respect to pressure).

Our calibrated Crushable Foam model will give priority to ensuring accuracy, or at least conservatism, of the initial yield surface rather than post-yield behavior (i.e. hardening). The Abaqus Crushable Foam material model incorporates a flow rule such that under proportional loading the direction of flow is identical to the direction of stress. Abaqus also allows a choice of volumetric hardening, in which the material hardens with compressive pressure (the ellipse grows only in the positive pressure direction), and

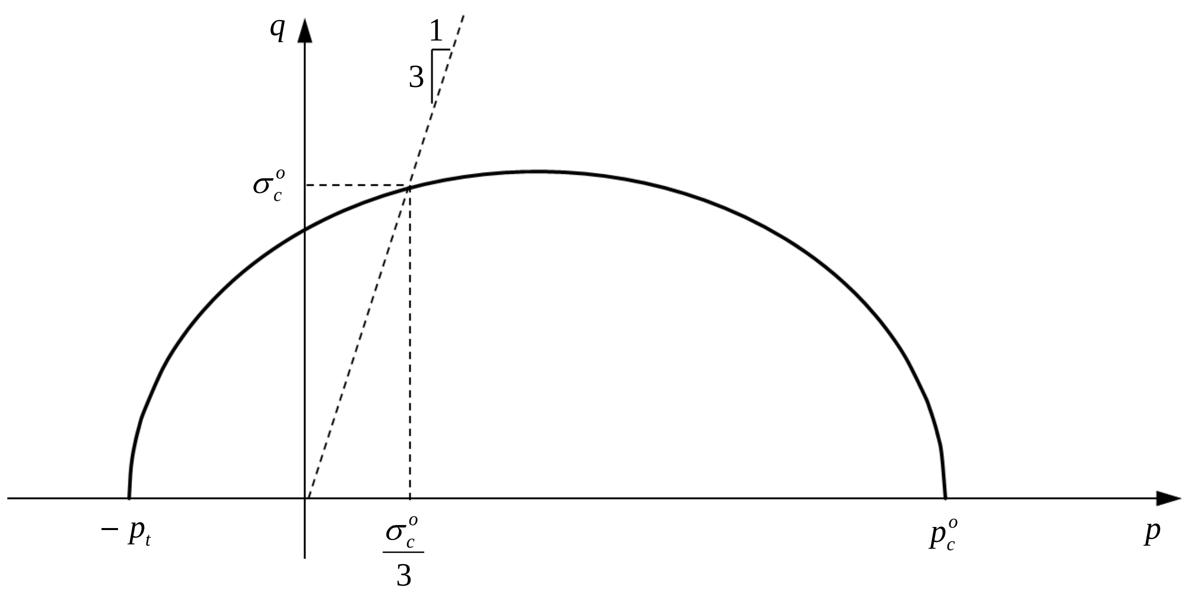

Figure 1. Elliptical yield surface used in the Abaqus Crushable Foam material model. σ_c^o is the uniaxial compressive yield stress and p_c^o and p_t are the compressive and tensile pressure stress, respectively, that cause initial yield.

isotropic hardening, in which the yield surface grows symmetrically about the center of the ellipse. We assume no hardening, which is intended to be a conservative assumption in light of the variability in post-yield behavior displayed by the material (this can be seen in the plots discussed in section 4.3).

Material parameters required by Abaqus for the Crushable Foam model are the yield stress ratio, k, for compression loading, defined as the ratio of initial yield stress in uniaxial compression to the initial yield stress in hydrostatic compression, and the yield stress ratio, k_t, for hydrostatic loading, defined as the ratio of the yield stress in hydrostatic tension to the yield stress in hydrostatic compression. Thus, we require the two points, p_t and $p_c{}^o$, at which the elliptical yield surface intersects the pressure axis and the point, $\sigma_c{}^o$, at which a line from the origin of slope 1/3 (the ratio of pressure to Mises stress) intersects the ellipse.

3 Available test data

The primary source of test data used for model calibration is an extensive study of the effect of pressure on APO-BMI plasticity performed by UNM at the request of Matt Lewis in 2004. The material used for these tests did not originate from a war reserve billet, so a secondary series of tests, performed only under uniaxial compression, was performed by W-14(Kingston, 2013) to confirm that the material used by UNM adequately represented the war reserve material.

In the UNM tests hydraulic fluid was used to pressurize the cylindrical specimen (nominally 2.8 in. long and 1.4 in. in diameter). While under constant confining pressure, a load frame applied an axial compressive load at a constant displacement rate up to and beyond yield and failure. Both axial and transverse strains were measured. Confining pressures of 0psi (i.e., uniaxial), 50psi, 100psi, 300psi, 500psi, 650psi, and 800psi were used. Purely hydrostatic tests (i.e. without the load frame superimposing the additional axial load) were also conducted. Between one and five replicates were tested at each condition. Three tensile specimens were also tested, but failure occurred outside the gage section, and there was significant scatter, so it is believed that bending stresses caused artificially low failure loads compared to true uniaxial behavior. All tests are described in detail in (Reser, Ahuja, & Lenke, 2004), and the results are summarized in Table 1.

The W-14 tests used the same nominal specimen geometry as the UNM tests and attempted to reproduce the UNM uniaxial compression tests, except that only axial strains were measured. In general, the W-14 tests showed less scatter than the UNM tests, and the average initial yield strength was higher but within the distribution of the UNM tests. The W-14 tests are described in detail in (Kingston, 2013), and the results are summarized in Table 2.

Specimen ID	*Test pressure (psi)*	*Pressure at yield (psi)*	*Mises stress at yield (psi)*	*Bulk modulus (psi)*	*Shear modulus (psi)*	*Young's modulus (psi)*	*Poisson's ratio*
TS50-34	50	313.3	795.0	74859	53583	129784	0.211
TS50-3	50			68234	56107	132110	0.177
HYD-21	hydrostatic	1002.3	15.9	58091			
TS100-29	100	424.0	975.5	56849	52877	121088	0.145
TS300-4	300	572.0	812.4	56547	51340	118237	0.152
TS500-17	500	773.7	825.3	67654	58468	136175	0.165
TS650-12	650	809.2	481.1	67609	48035	116513	0.213
TS800-25	800	914.6	348.5	56378	52591	120352	0.144
HYD-31	hydrostatic	936.5	14.4	59985			
HYD-9	hydrostatic	1075.6	42.2	55910			
UNIAXL-22	0	255.3	752.5	58920	59325	133253	0.123
UNIAXL-11	0	268.7	796.9	47259	63281	131258	0.037
UNIAXL-18	0	404.9	1205.6	66348	59563	137534	0.155
UNI-8	0	258.1	770.2	57097	50184	116438	0.160
TS300-H-1	300	589.3	868.0	62475	50744	119799	0.180
TS500-H-15	500	743.0	728.0	65464	64899	146338	0.127
TS650-H-33	650	835.0	554.2	65023	50467	120283	0.192
TS800-H-26	800	912.3	346.4	62117	44718	108192	0.210
TS300-D-27	300	529.3	690.1	55815	48394	112630	0.164
TS500-D-20	500	721.5	665.6	56749	50628	117069	0.156
TS650-D-14	650	865.1	640.9	66776	58539	135904	0.161
TS800-D-35	800	909.5	328.6	60124	41423	101061	0.220
HYD-7	hydrostatic	946.7	-6.0	58624			
HYD-36	hydrostatic	1138.5	11.2	61232			
TS800-23	800	921.3	375.4	63241	58698	134485	0.146
			mean	**61175**	**53693**	**124425**	**0.162**
			Std Dev	**5744**	**6071**	**11400**	**0.041**

Table 1. Summary of UNM test data. Note that the test number is given in the last one or two digits of the specimen name.

Specimen ID	*Test pressure (psi)*	*Pressure at yield (psi)*	*Mises stress at yield (psi)*	*Young's modulus (psi)*
B-2	0	416.4	1249.1	129880
A-2	0	425.4	1276.3	125380
C-2	0	390.0	1170.1	124950
C-1	0	419.7	1259.0	128050
A-1	0	402.0	1206.1	130500
			mean	**127750**
			Std Dev	**2532.1**

Table 2. Summary of W-14 test data.

4 Regressing the test data and estimating the model parameters

4.1 Data regression

The parameters to be extracted from the available test data are the two elastic constants and the initial yield stress, in terms of the Mises stress, as a function of pressure to which an elliptical yield surface, such as that shown in Figure 1, can be fit. Although the elastic parameters and yield pressures for the UNM tests were estimated by Lewis (Lewis, 2004), the process was repeated again in the current work to ensure traceability. Lewis found the Young's modulus and shear modulus to be 129.9 ksi and 53.9 ksi, respectively, which result in a Poisson's ratio of 0.205. Note that, consistent with the previous work, we are fitting the model to only the UNM data; the W-14 data is used to demonstrate that the material used by UNM is representative of WR material.

In the current work, the shear modulus was estimated by fitting a line to two points on the shear stress versus shear strain curve. Similarly, the bulk modulus was estimated by fitting a line to two points on the pressure versus compressive volumetric strain curve. In almost all cases the two points were the point at which the stress was closest to 50psi and the point at which the stress was closest to 75% of the maximum stress. For three of the bulk modulus calculations on uniaxial tests different points were chosen to accommodate anomalies in the data: for test UNI-8 (see Table 1 for a list of the tests) the second point was 65% of the maximum pressure, for test UNIAXL-11 the minimum stress was 110psi, and for test UNIAXL-18 the minimum stress was 150psi.

The lines fit to the data can be seen in the plots provided in Appendix A, and the values of bulk and shear modulus, which are within 5% and 0.5%, respectively, of the values estimated by Lewis, are summarized in Table 1. The Young's modulus and Poisson ratio given in Table 1 are calculated from the shear and bulk modulus. It is also possible to estimate the Young's modulus by fitting the initial slope of the axial stress versus axial strain curve in the uniaxial tests using the same method as described above for the shear and bulk modulus. Doing this results in an average Young's modulus of 142 psi, which is 14% higher than the value estimated from the bulk and shear modulus shown in Table 1. The reason for this difference has not been investigated, and considering the relatively large standard deviations reported in Table 1, the elastic properties of this material should be treated as distributions in analyses where accuracy of these material properties is important.

There are several possible methods for extracting the yield stress from the stress-strain data produced by the UNM tests. An offset method, similar to the familiar 0.2% offset method used in metals, was attempted, but it proved difficult to obtain values that agreed with intuition when using the same offset strain for all data. The most successful method, and the method used for the results reported here, determined the yield point as the pressure that deviated sufficiently from a straight line fit to the linear portion of the pressure-volumetric strain curve[1]. Note that because initial yield is, in some tests, followed by subsequent elastic response with a stiffness similar to the initial stiffness, this method results in a conservative estimate of yield stress. Plots showing the yield point determined by this method for each test are given in Appendix A.

4.2 Model parameter estimation

The elastic parameters are taken to be the averages shown in Table 1; i.e., the Young's modulus is 124ksi (858MPa) and the Poisson ratio is 0.16. The parameters, k, k_t, and σ_c^o describing the yield surface are determined by constructing the largest possible yield surface in p-q space which does not contain any of the experimental data points. This yield surface is shown, along with the test data from Table 1 and Table 2, in Figure 2. Also shown in this figure is a yield surface not intended to provide conservative strength, but rather intended to more closely fit the average strength observed in the tests. Note that because of the limited number of test data points, statistical distributions of the data

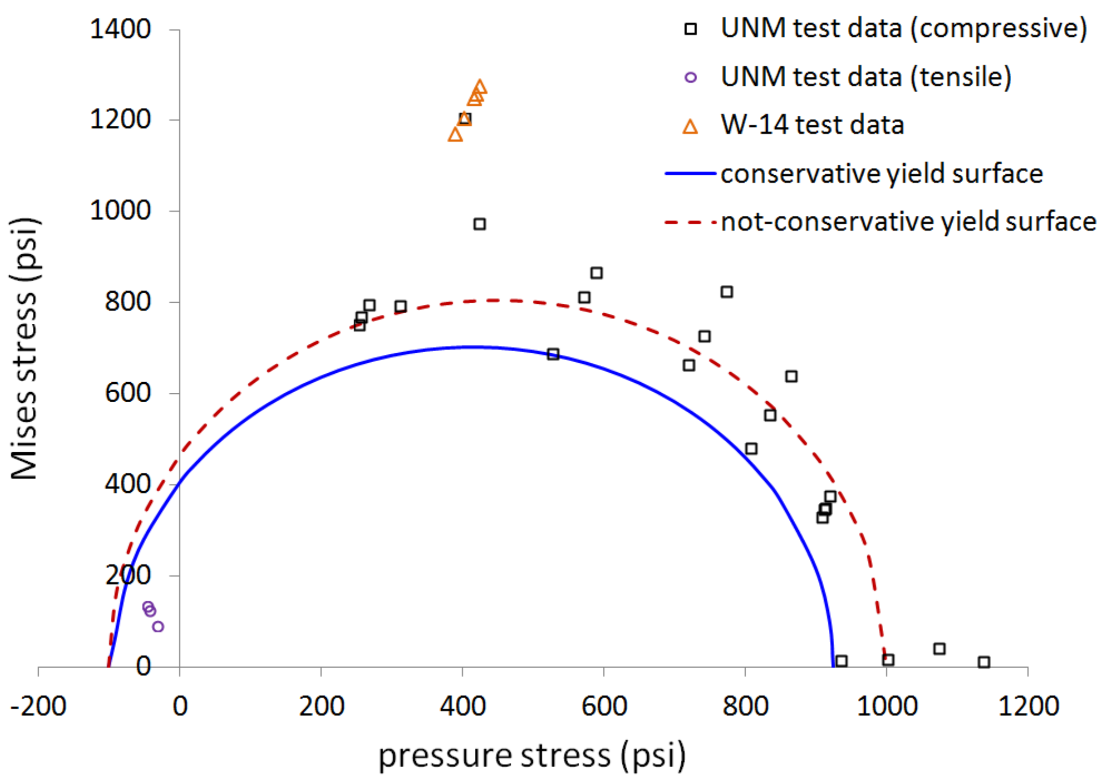

Figure 2. Two yield surfaces constructed to represent the UNM test data: one intended to be conservative, and one, labeled not-conservative, intended to be more representative of the mean test data.

[1] To eliminate the need to filter noise, which would cause false-detection of the deviation of the data from the line, the data was searched from highest strain to lowest for the pressure that first met the line to within a predefined tolerance. A tolerance of 2% was used for every UNM test.

Model parameter	*Conservative model*	*Not-conservative model*
Young's modulus, E (MPa)	858	858
Poisson's ratio	0.162	0.162
k	0.7	0.75
k_t	0.1	0.1
σ_o^c (MPa)	4.45	5.17

Table 3. Model parameters used for the conservative and not-conservative yield surfaces.

points were not determined, and the not-conservative yield surface is merely an "eyeball fit" to the data. Similarly, the conservative yield surface was determined by adjusting the model parameters until the ellipse appeared to fall just inside the compressive data. Applying more rigor in these fits may be possible and should be attempted if analyses show sensitivity to this yield surface.

In both yield surface estimates, the tensile data is ignored due to the data being suspect. Furthermore, following the suggestion given in section 19.3.5 of the Abaqus Analysis User's Manual (Dassault Systèmes Simulia Corp, 2009), k_t was taken to be 10% in all cases.

The parameters used for each of the two yield surfaces are listed in Table 3. Note that only k and σ_o^c differ between the two.

4.3 Model verification

In this section we verify that the model is behaving as intended. Single-element bilinear axisymmetric Abaqus models of the UNM tests were constructed using the parameters shown in Table 3. Note that there is no hardening assumed for either model.

Loading in the verification models is intended to simulate the loading of the tests. There are two steps: in Step 1 a uniform pressure is applied to the element's external surfaces, and in Step 2, while maintaining the uniform and constant pressure, a compressive displacement is applied to the element's top surface with the bottom surface axially constrained. For the six models simulating the six general triaxial cases the pressures are set to 50psi, 100psi, 300psi, 500psi, 650psi, and 800psi to mimic the test pressures. For the purely hydrostatic case, Step 2 is omitted, and the pressure in Step 1 is set to be larger than the hydrostatic compressive yield pressure. Note that in this case the model is in load control and, since there is no hardening, does not run to completion. In the uniaxial case Step 1 is omitted.

The resulting failure loci for the conservative and not-conservative models are shown in Figure 3. Note that for the loadings considered the Tresca stress (twice the maximum shear stress) is equal to the Mises stress. These results illustrate that the yield surfaces shown in Figure 2 are being obeyed by the material model. The stress-strain plots from which Figure 3 was derived are provided in Appendix B.

Uniaxial stress-strain behavior of the model is compared to the uniaxial tests performed by both UNM and W-14 in Figure 4. Note that both the conservative (Figure 4(a)) and not-conservative (Figure 4(b)) material models have lower yield strengths than all the test data. This is consistent with the data displayed in Figure 2 since the uniaxial tests, which correspond to the points closest to 2MPa in Figure 3, are in the region of the yield surface where both material models are the most conservative. It is also apparent that the W-14 tests represent stronger material than the UNM tests. This may be because the W-14 tests were performed on a WR-quality billet while the UNM tests were performed on material manufactured specifically for the tests.

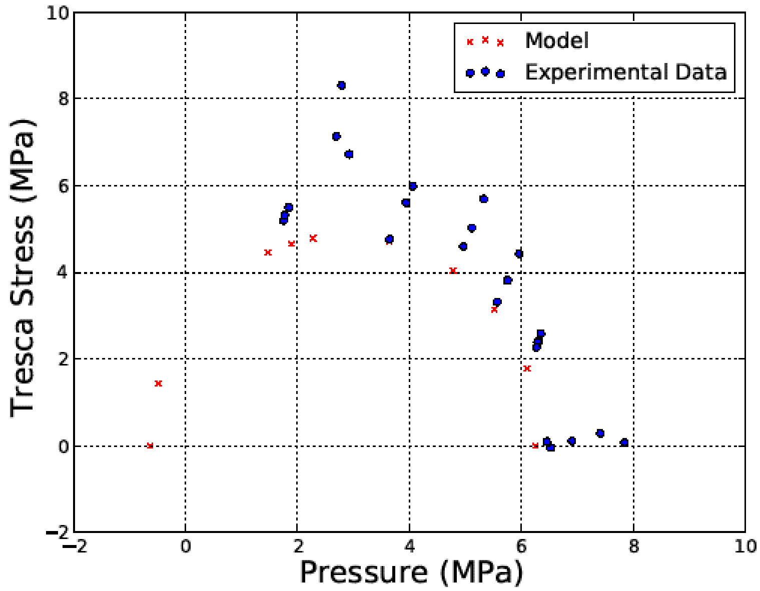

(a)

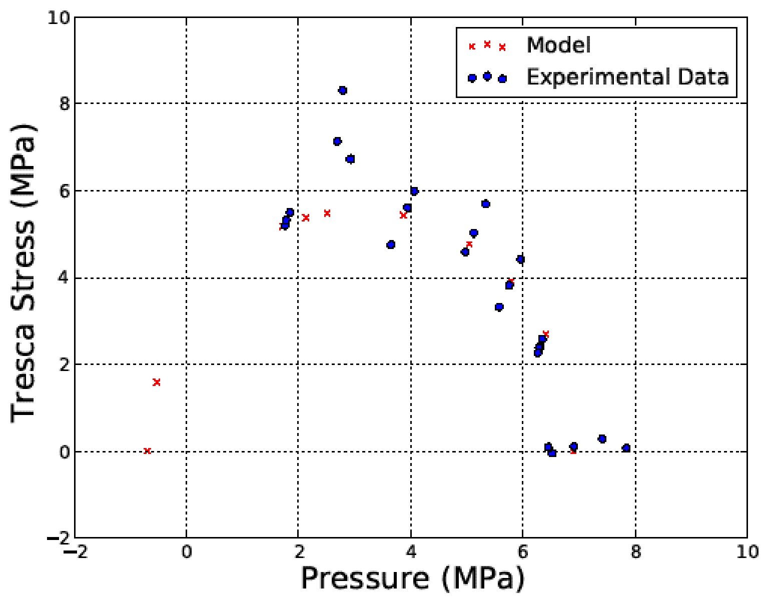

(b)

Figure 3. Comparison of failure locus in Tresca-pressure space for (a) the conservative material model and (b) the not-conservative material model.

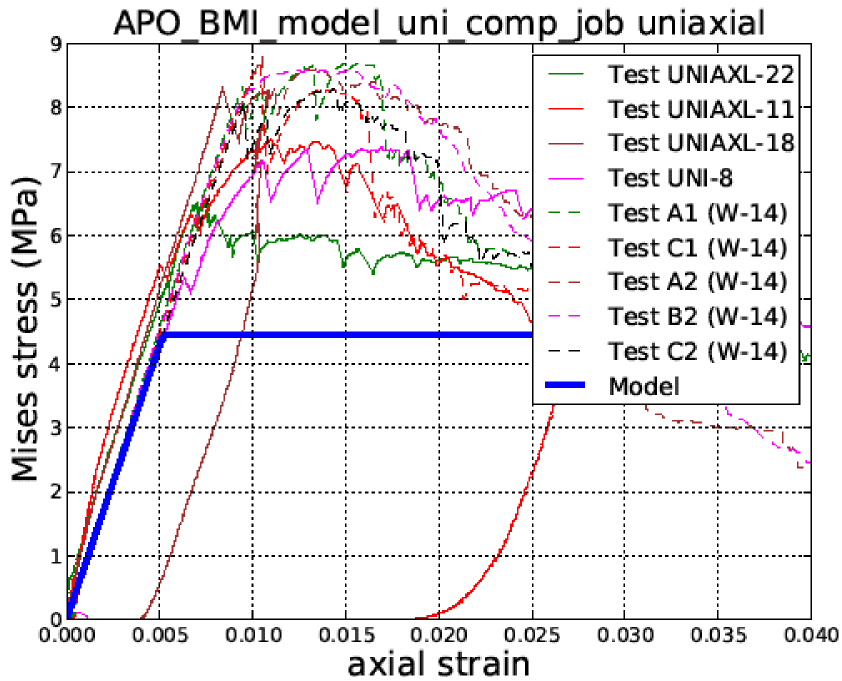

(a)

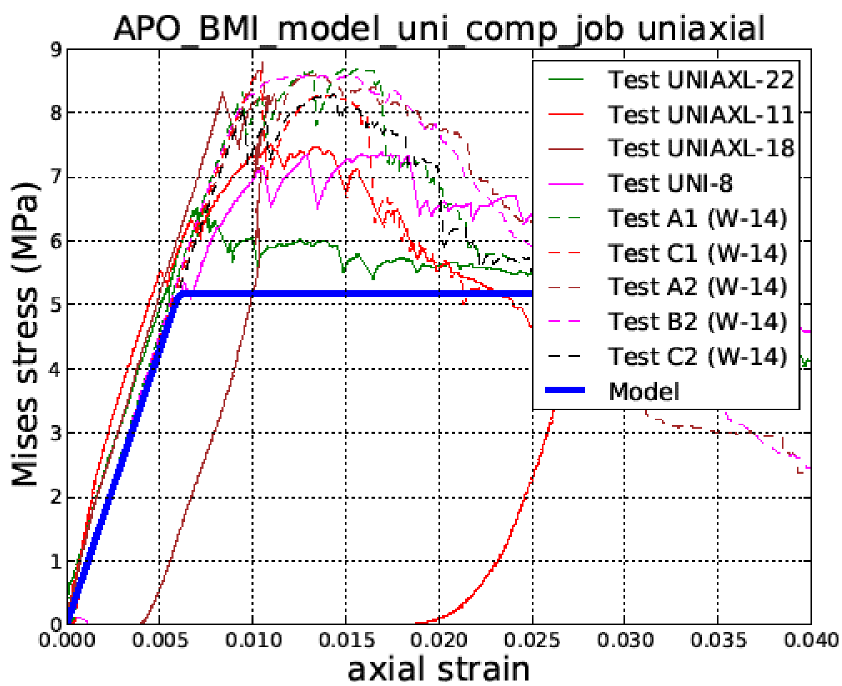

(b)

Figure 4. Uniaxial stress-strain behavior of (a) the conservative and (b) the not-conservative models compared to both the UNM and W-14 uniaxial tests.

5 Conclusion

The Abaqus material models of APO-BMI with carbon microballoons calibrated in this report are given in Table 4. It has been verified that, under the loading conditions of the tests to which the models were calibrated, the models perform as intended and represent either a conservative (for the conservative model) or a more representative (for the not-conservative model) strength of the material. Behavior beyond initial yield is not captured accurately in the models, although as Appendix B shows the model is generally conservative for a considerable amount of straining after yield. If applications of these models are sensitive to post-yield behavior then these models will be inadequate. Furthermore, when calculations are sensitive to either the elastic parameters or yield stress of this material, statistical distributions should be estimated.

Conservative model	*Not-conservative model*
*MATERIAL, NAME=APO-BMI *Elastic 858., 0.162 *Crushable Foam 0.7, 0.1 *Crushable Foam Hardening 4.45,0. 4.45,1.	*MATERIAL, NAME=APO-BMI *Elastic 858., 0.162 *Crushable Foam 0.75, 0.1 *Crushable Foam Hardening 5.17,0. 5.17,1.

Table 4. *Material cards used in the Abaqus verification models.

References

Dassault Systèmes Simulia Corp. (2009). Abaqus Analysis User's Manual (V6.9). Providence, RI, USA: Dassault Systèmes Simulia Corp.

Kingston, L. (2013). *W-14-TR-0118U: APO-BMI Foam Compression Test Report (draft).* LANL.

Lewis, M. (2004). *ESA-WR:04-215: Model Fit for APO-BMI Syntactic Foam.*

Reser, P. M., Ahuja, N., & Lenke, L. R. (2004). *Characterization of Shear Properties for APO/BMI Syntactic Foam.*

Appendix A

This appendix contains plots of the volumetric and shear stress-strain data for each of the UNM tests showing the linear fit to the elastic region and the estimated yield point (as the intersection of the pressure stress with the volume strain at deviation). The plots are presented in the order of increasing applied pressure followed by the hydrostatic tests.

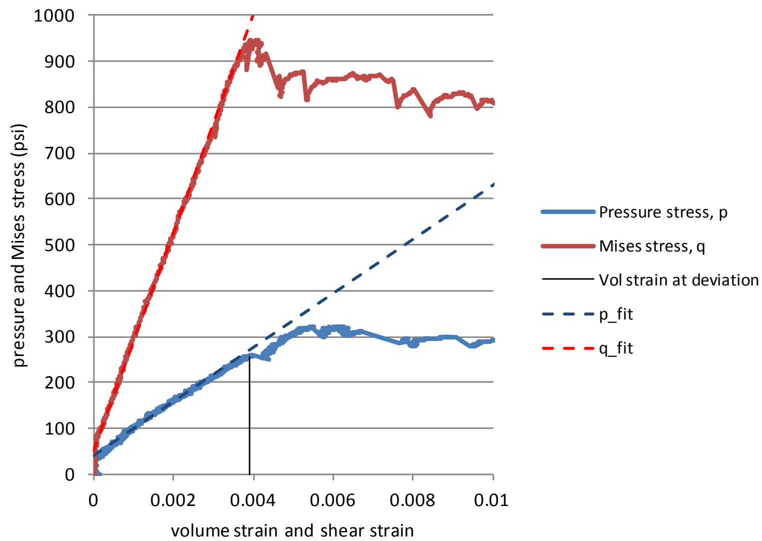

Figure A 1. Pressure and shear stress-strain for UNM specimen UNIAXL-22.

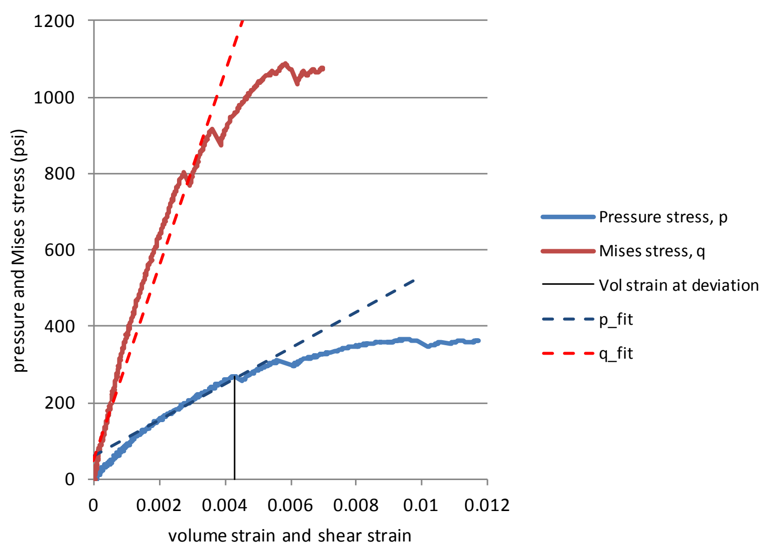

Figure A 2. Pressure and shear stress-strain for UNM specimen UNIAXL-11.

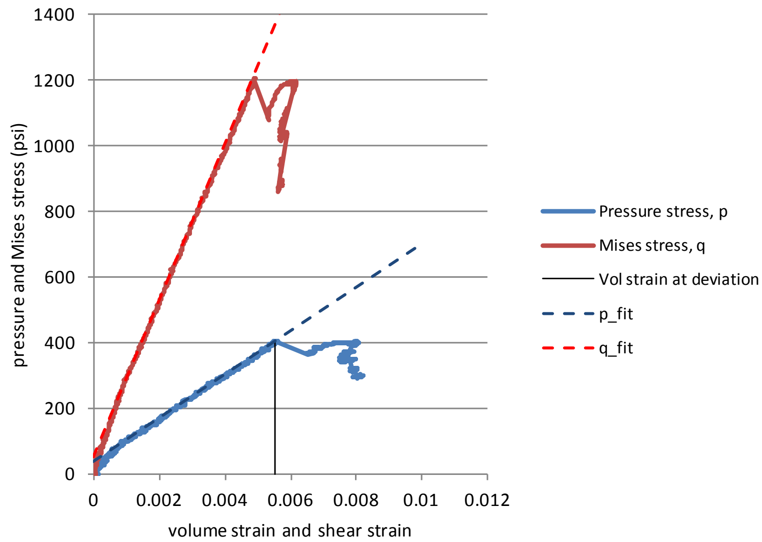

Figure A 3. Pressure and shear stress-strain for UNM specimen UNIAXL-18.

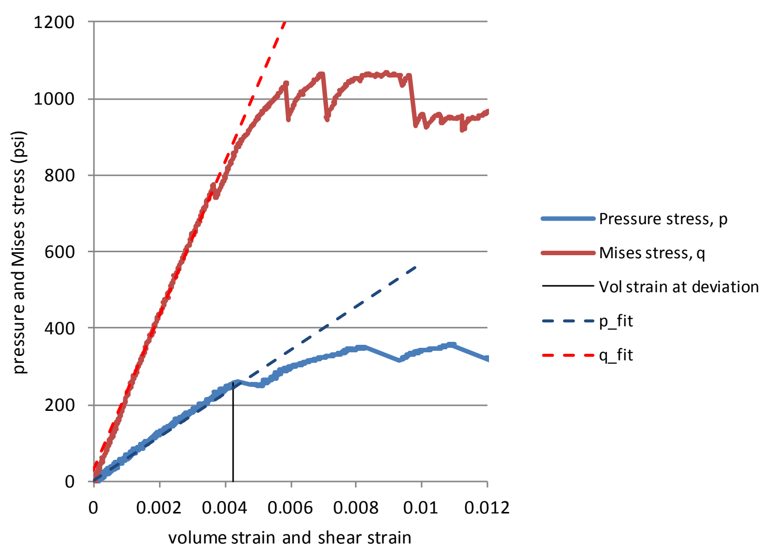

Figure A 4. Pressure and shear stress-strain for UNM specimen UNI-8.

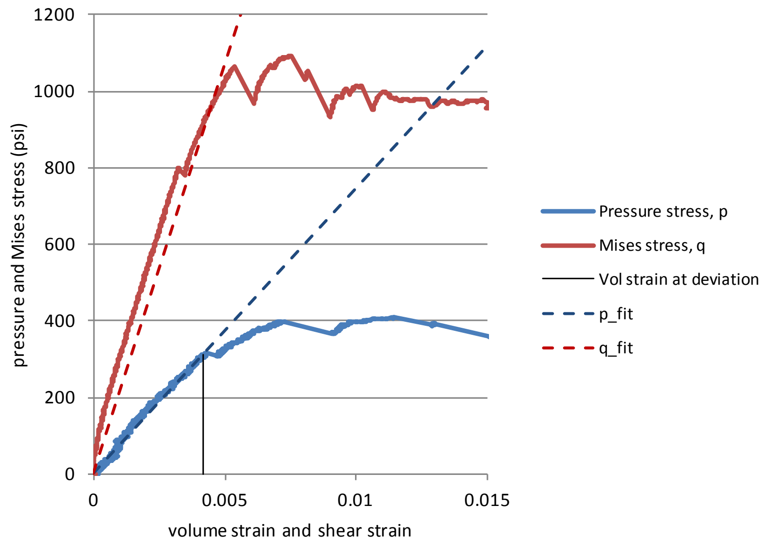

Figure A 5. Pressure and shear stress-strain for UNM specimen TS50-34.

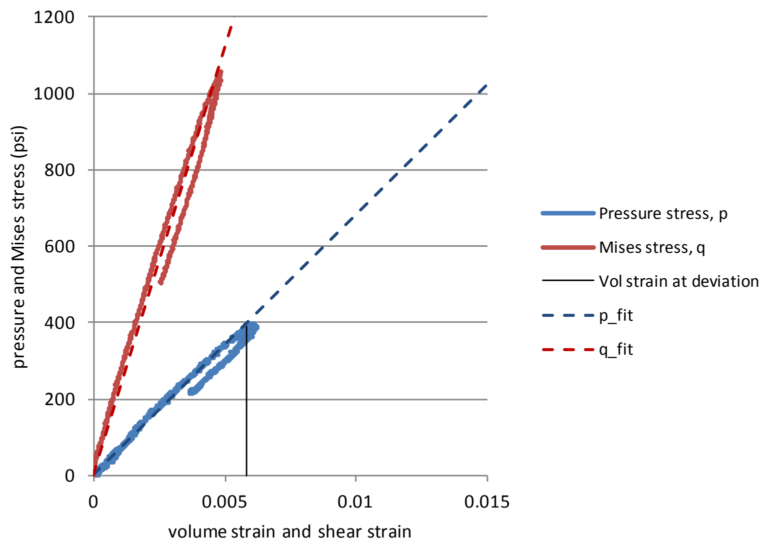

Figure A 6. Pressure and shear stress-strain for UNM specimen TS50-3.

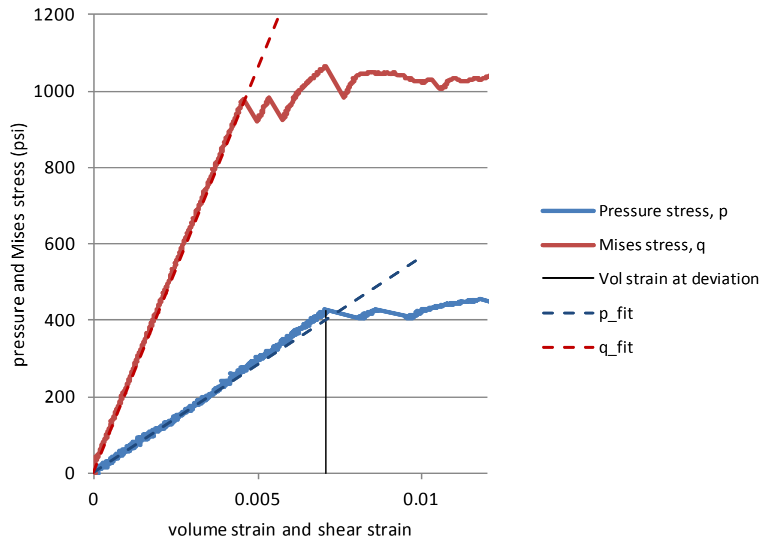

Figure A 7. Pressure and shear stress-strain for UNM specimen TS100-29.

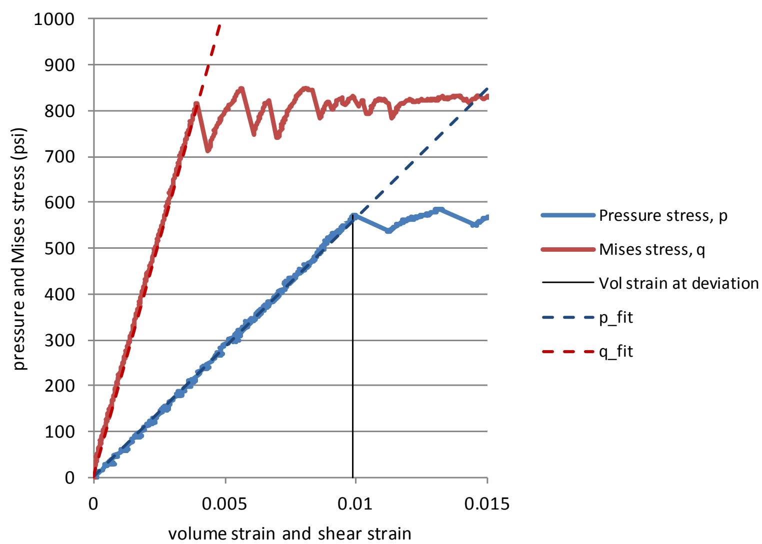

Figure A 8. Pressure and shear stress-strain for UNM specimen TS300-4.

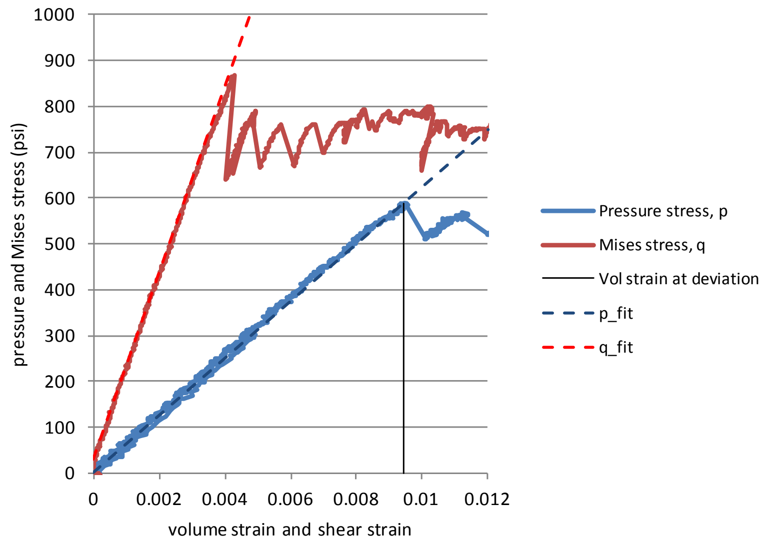

Figure A 9. Pressure and shear stress-strain for UNM specimen TS300-H-1.

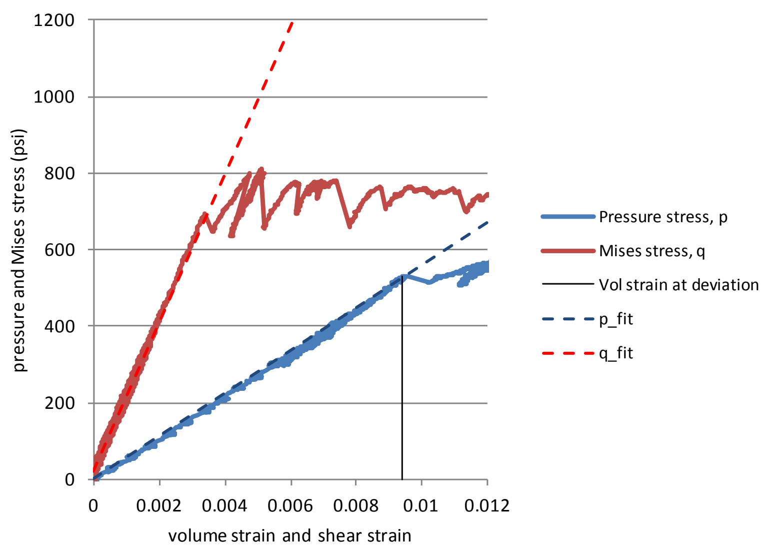

Figure A 10. Pressure and shear stress-strain for UNM specimen TS300-D-27.

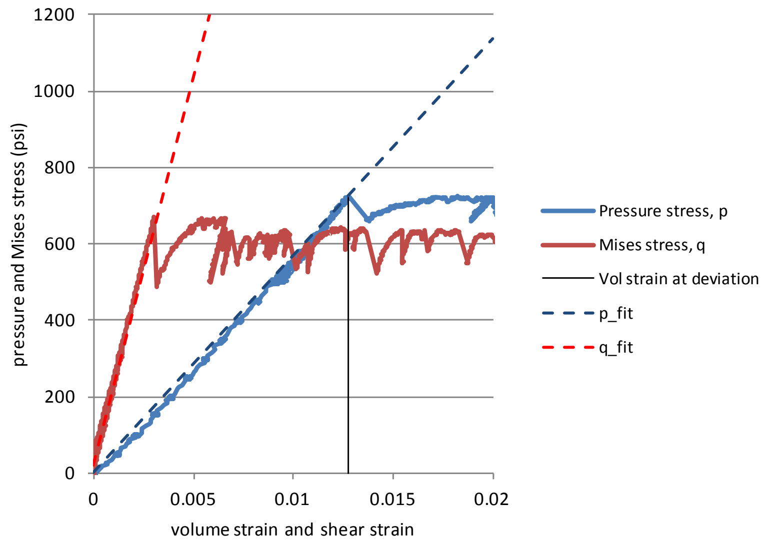

Figure A 11. Pressure and shear stress-strain for UNM specimen TS500-D-20.

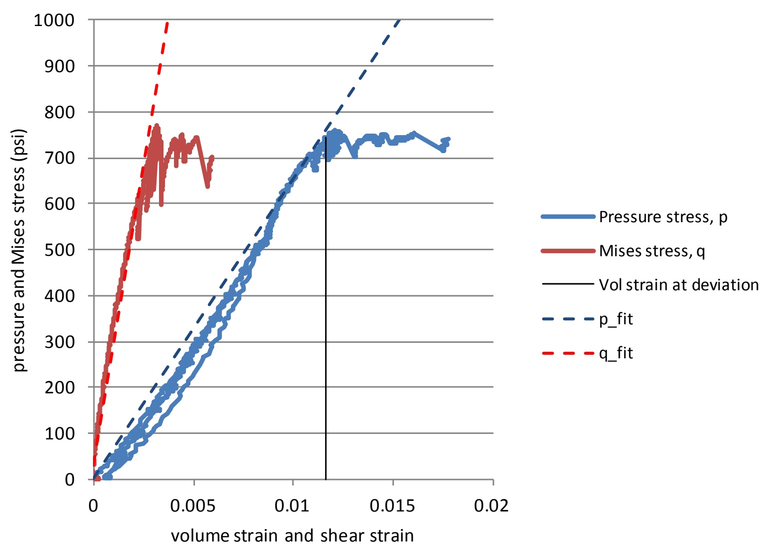

Figure A 12. Pressure and shear stress-strain for UNM specimen TS500-H-15.

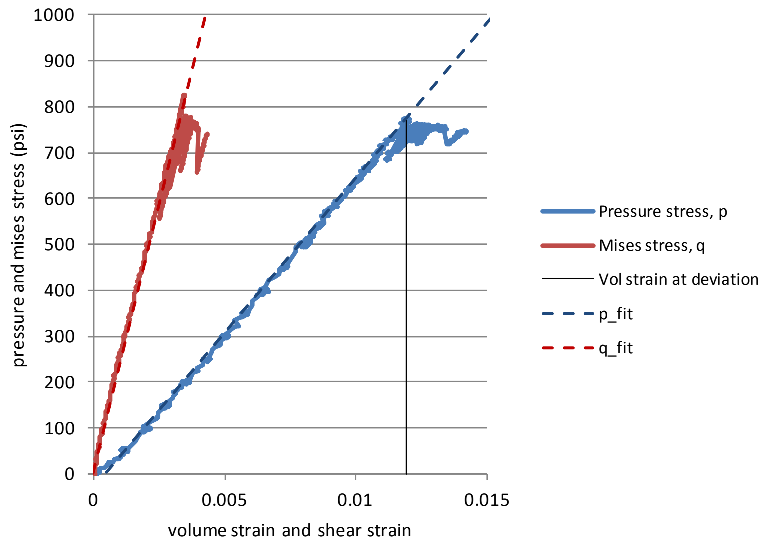

Figure A 13. Pressure and shear stress-strain for UNM specimen TS500-17.

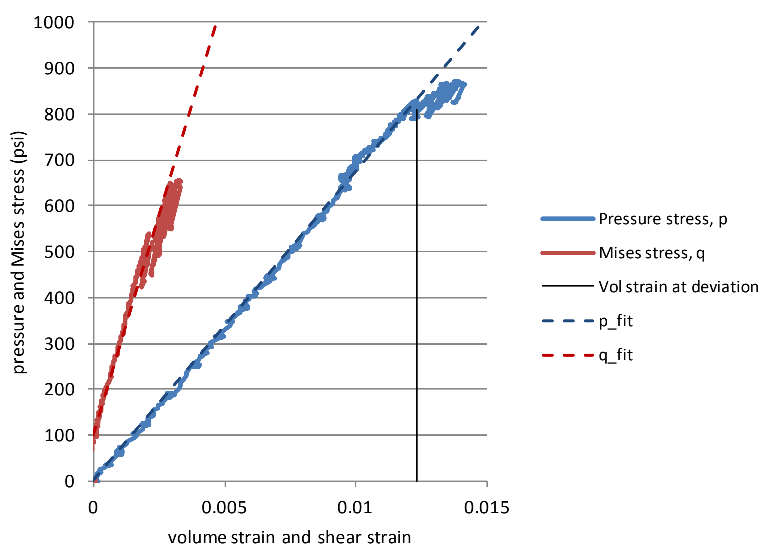

Figure A 14. Pressure and shear stress-strain for UNM specimen TS650-12.

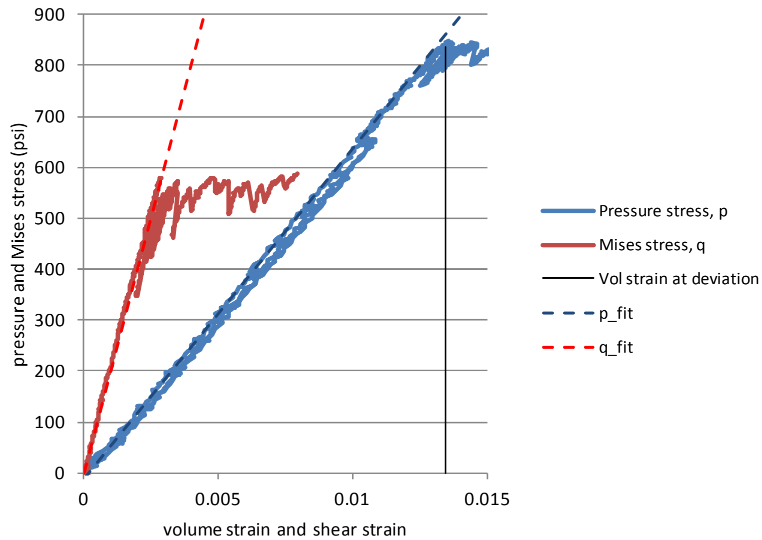

Figure A 15. Pressure and shear stress-strain for UNM specimen TS650-H-33.

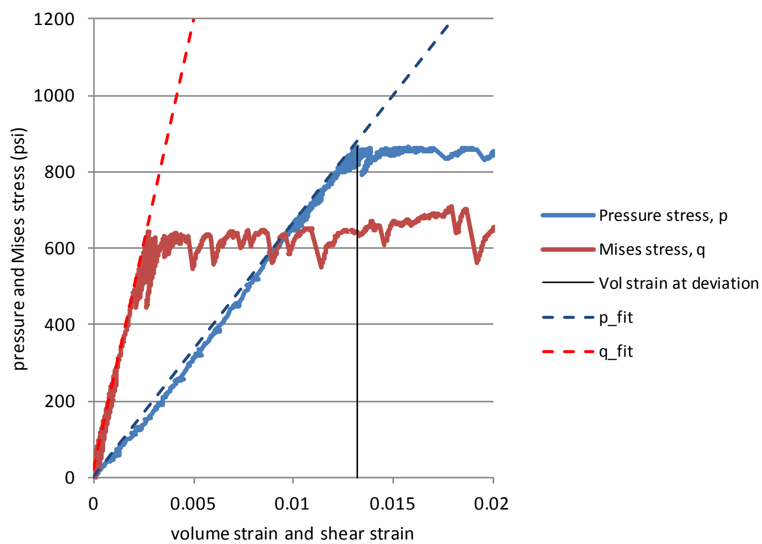

Figure A 16. Pressure and shear stress-strain for UNM specimen TS650-D-14.

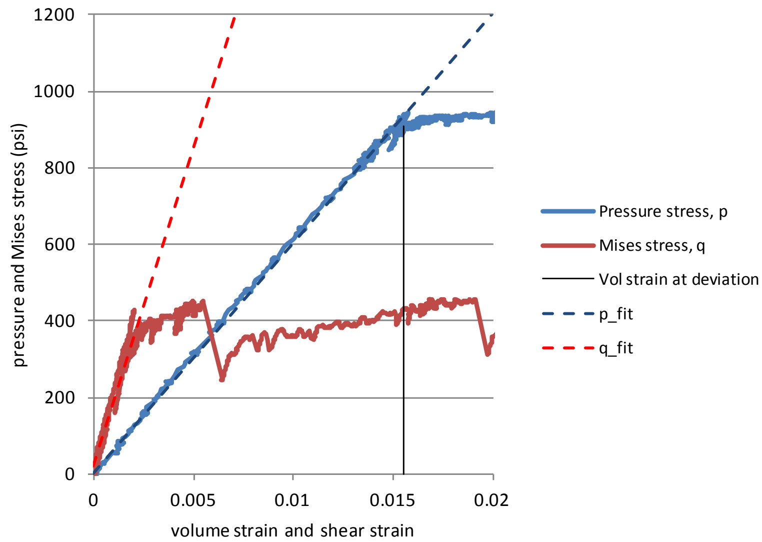

Figure A 17. Pressure and shear stress-strain for UNM specimen TS800-D-35.

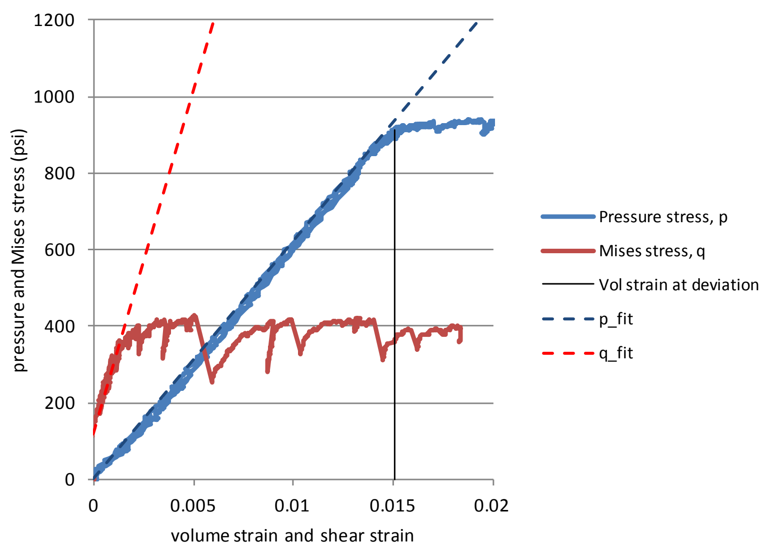

Figure A 18. Pressure and shear stress-strain for UNM specimen TS800-H-26.

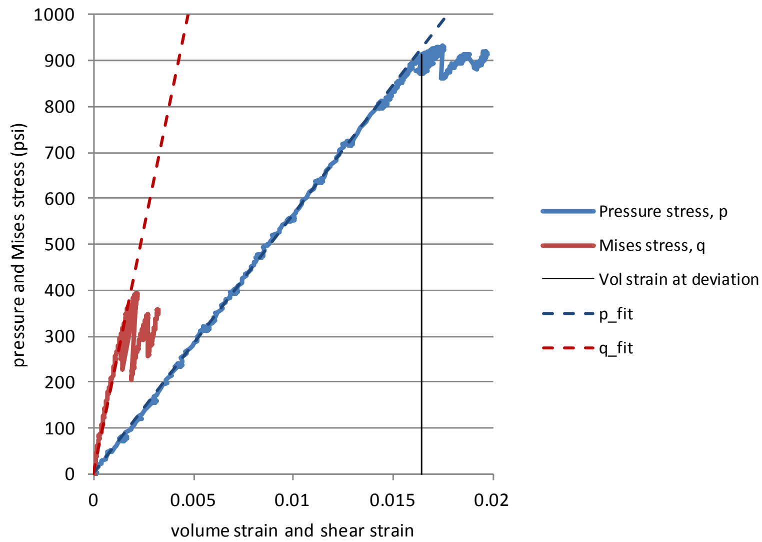

Figure A 19. Pressure and shear stress-strain for UNM specimen TS800-25.

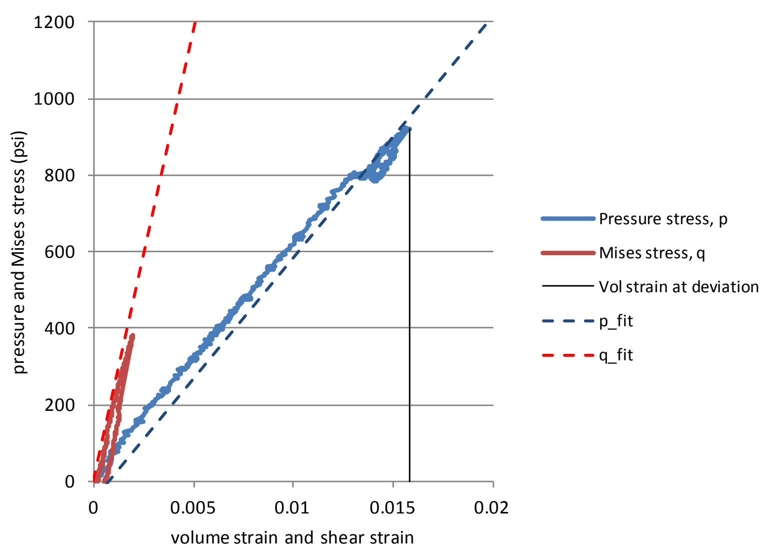

Figure A 20. Pressure and shear stress-strain for UNM specimen TS800-23.

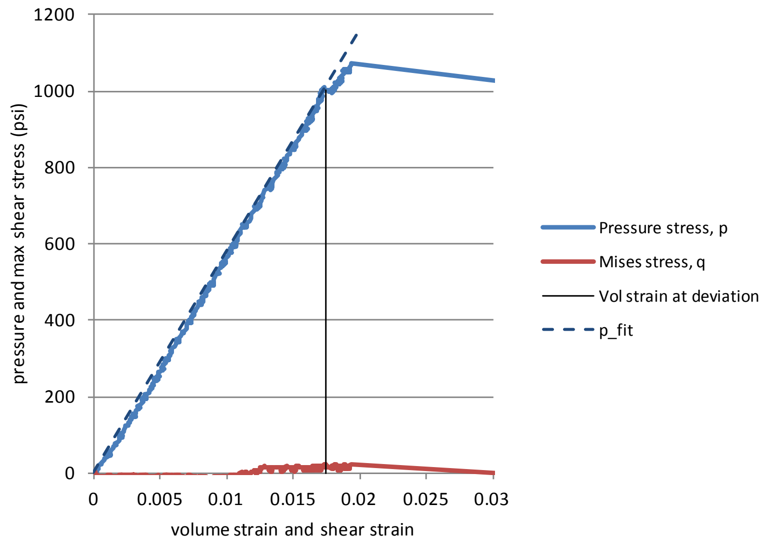

Figure A 21. Pressure and shear stress-strain for UNM specimen HYD-21.

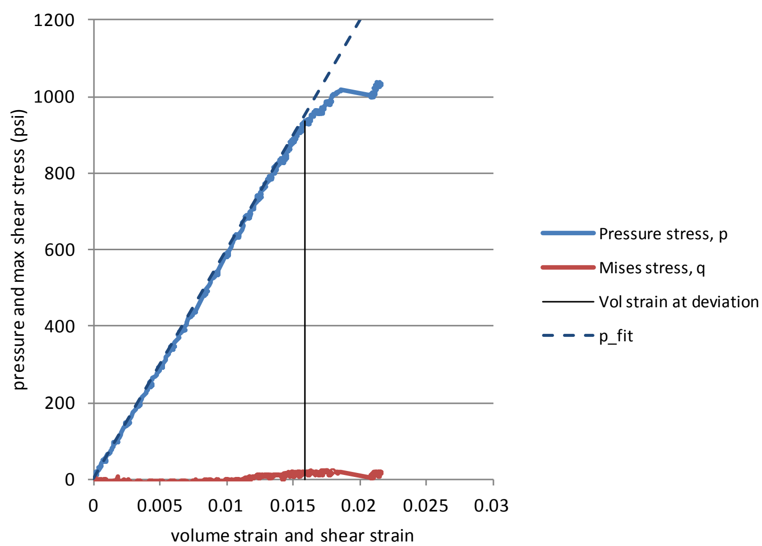

Figure A 22. Pressure and shear stress-strain for UNM specimen HYD-31.

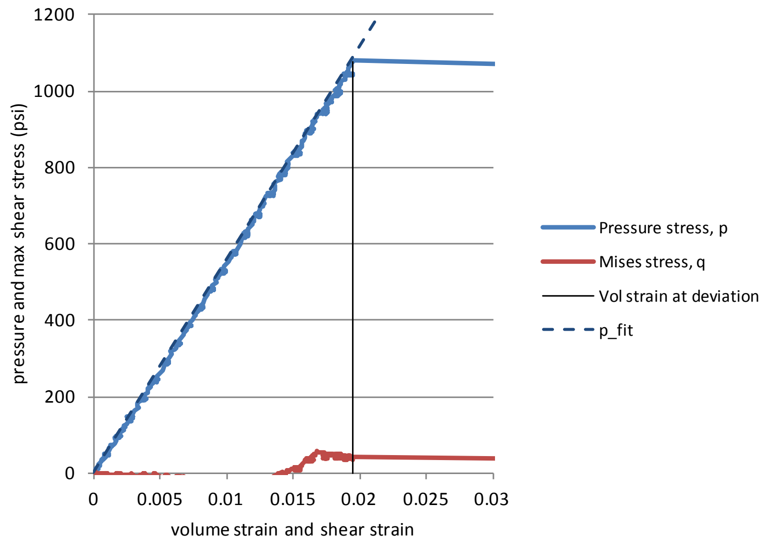

Figure A 23. Pressure and shear stress-strain for UNM specimen HYD-9.

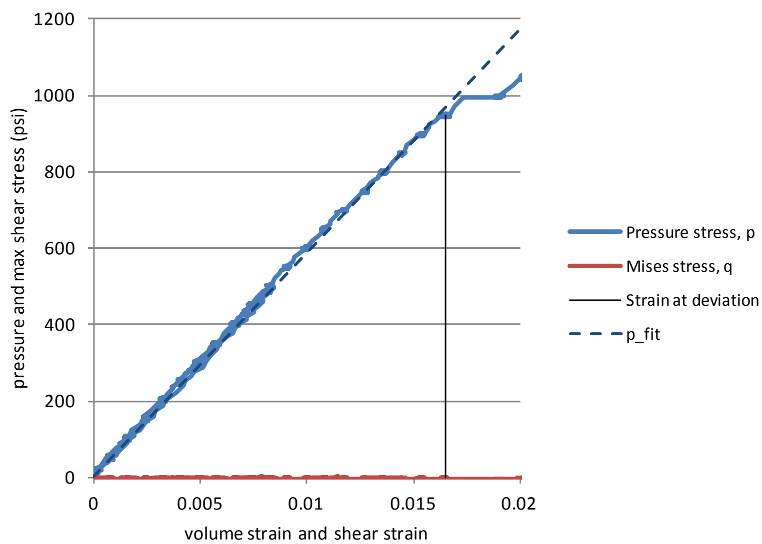

Figure A 24. Pressure and shear stress-strain for UNM specimen HYD-7.

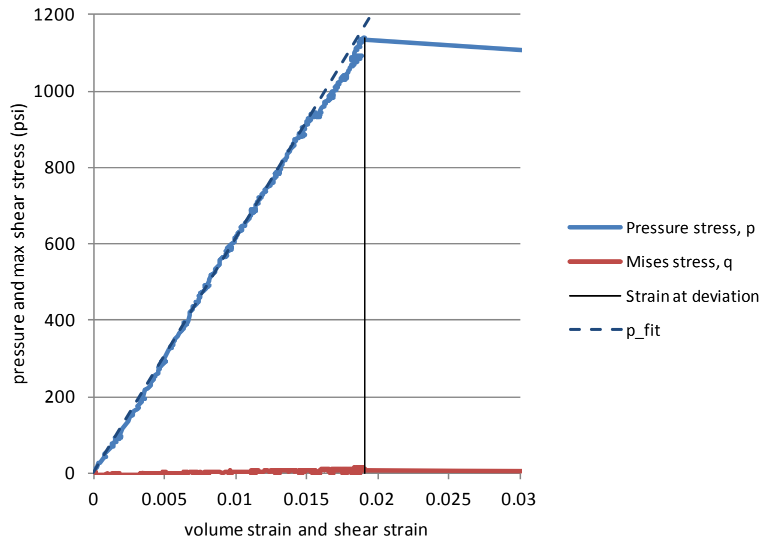

Figure A 25. Pressure and shear stress-strain for UNM specimen HYD-36.

Appendix B

This appendix contains a comparison of the test and model shear and volumetric stress-strain response for both the conservative and not-conservative material models. The plots are presented in the order of increasing applied pressure followed by the hydrostatic tests.

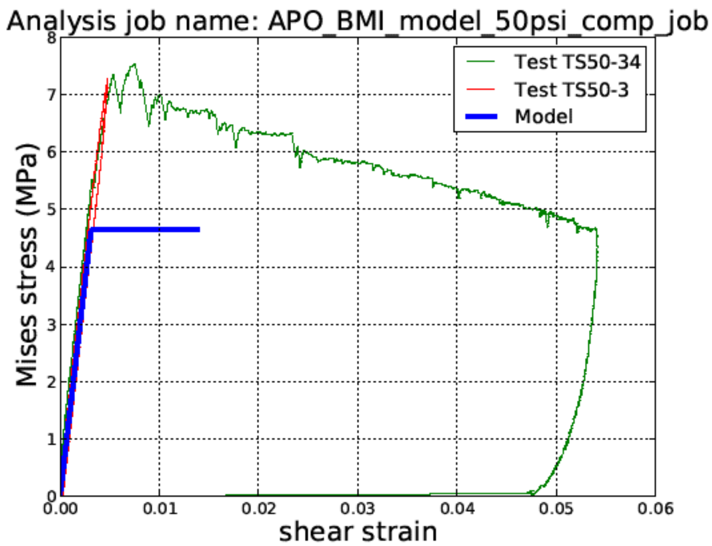

(a)

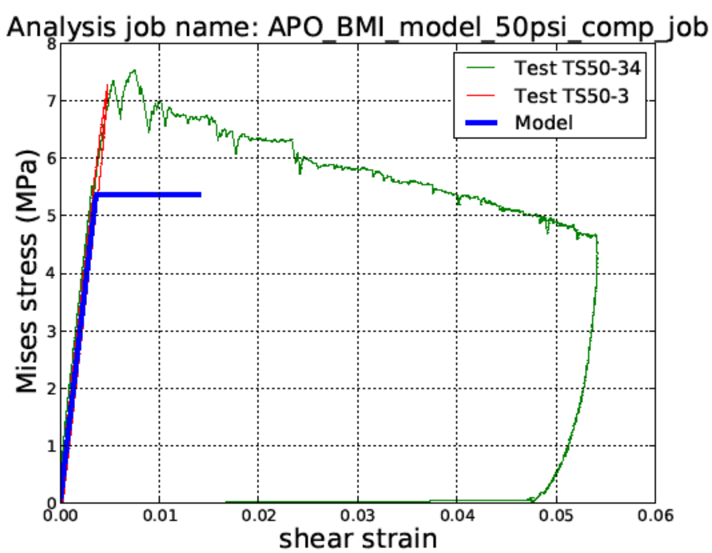

(b)

Figure B 1. Mises stress versus shear strain during axial compression with 50psi of pressure for (a) the conservative and (b) the not-conservative models compared to all UNM tests at this condition.

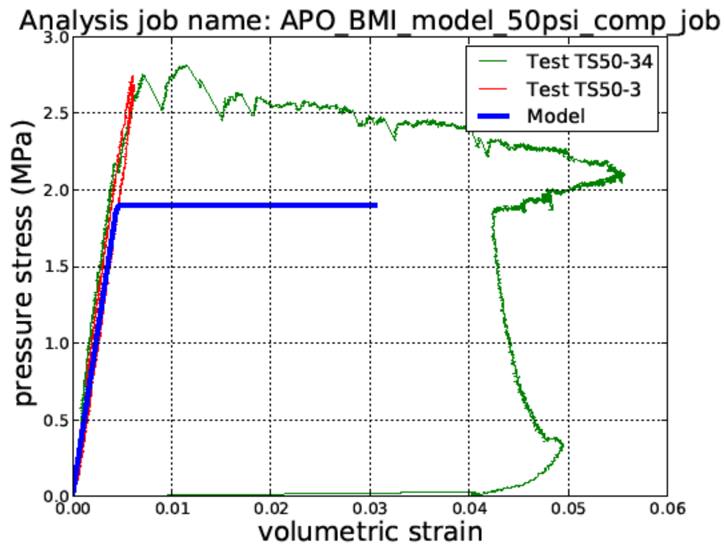

(a)

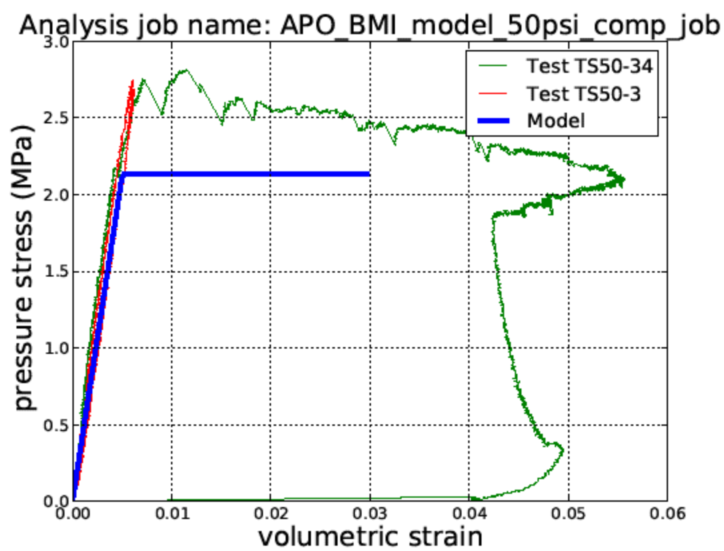

(b)

Figure B 2. Pressure stress versus volumetric strain during axial compression with 50psi of pressure for (a) the conservative and (b) the not-conservative models compared to all UNM tests at this condition.

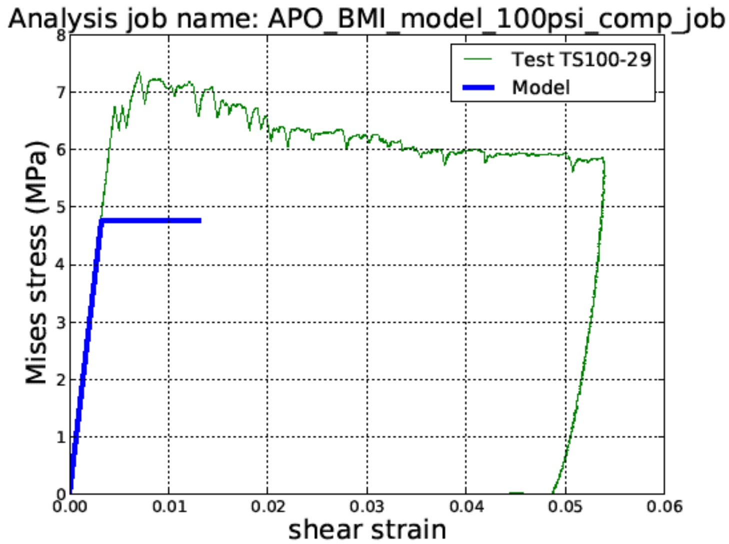

(a)

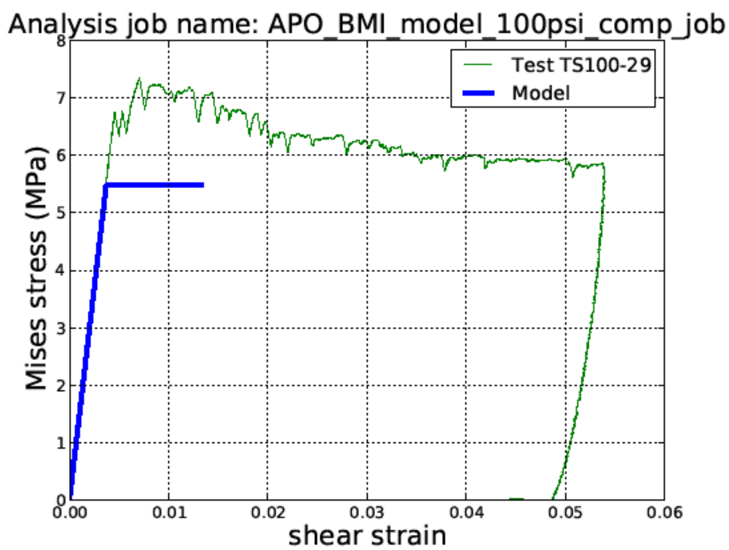

(b)

Figure B 3. Mises stress versus shear strain during axial compression with 100psi of pressure for (a) the conservative and (b) the not-conservative models compared to all UNM tests at this condition.

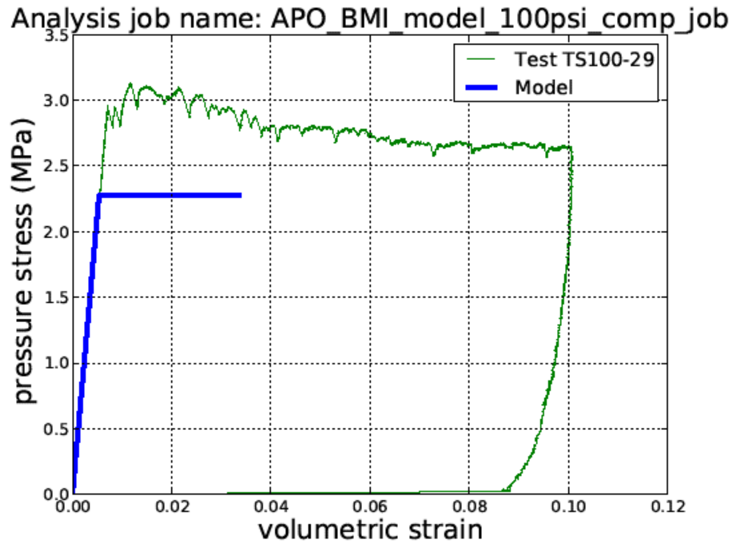

(a)

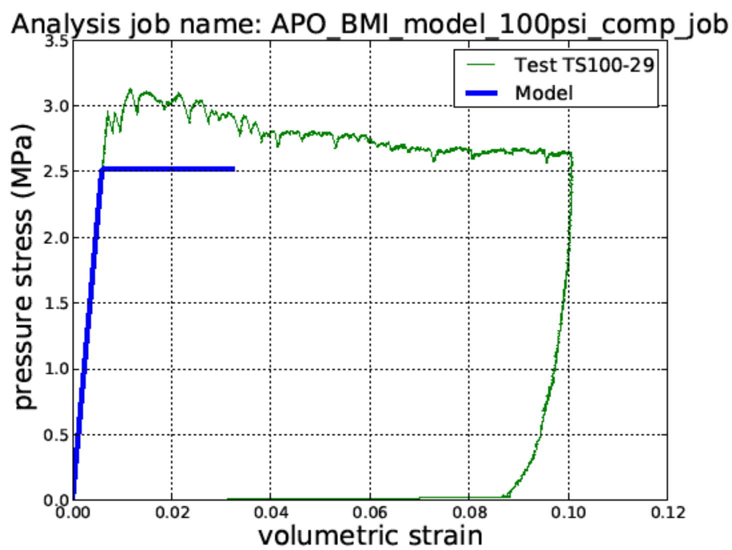

(b)

Figure B 4. Pressure stress versus volumetric strain during axial compression with 100psi of pressure for (a) the conservative and (b) the not-conservative models compared to all UNM tests at this condition.

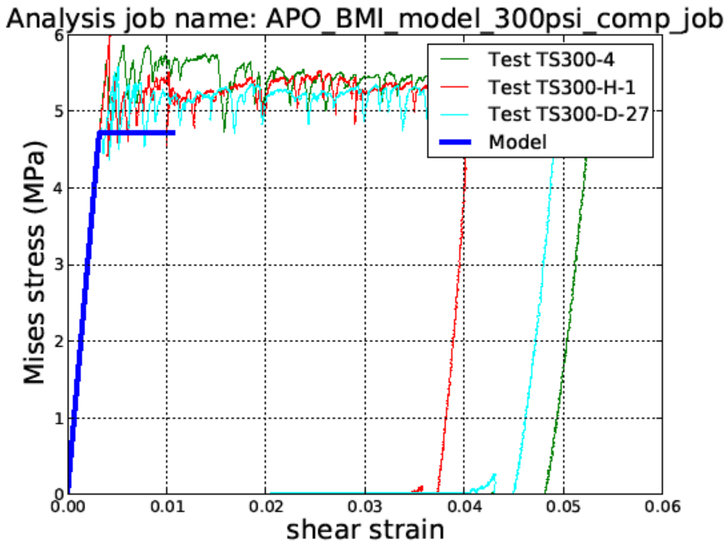

(a)

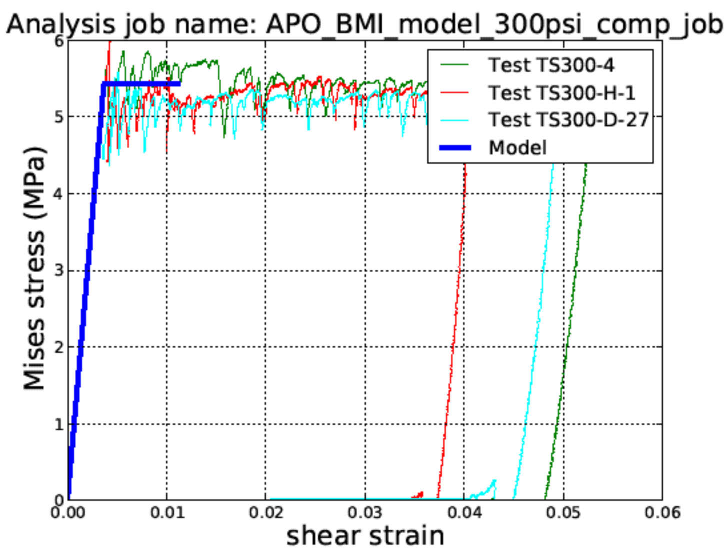

(b)

Figure B 5. Mises stress versus shear strain during axial compression with 300psi of pressure for (a) the conservative and (b) the not-conservative models compared to all UNM tests at this condition.

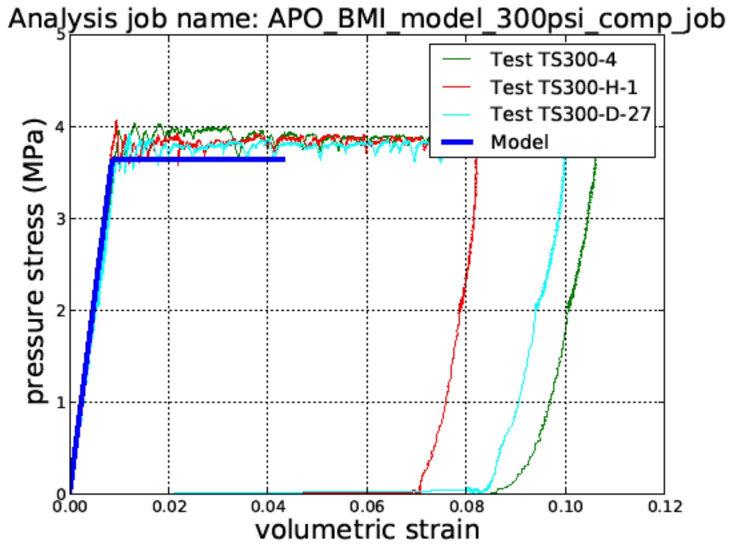

(a)

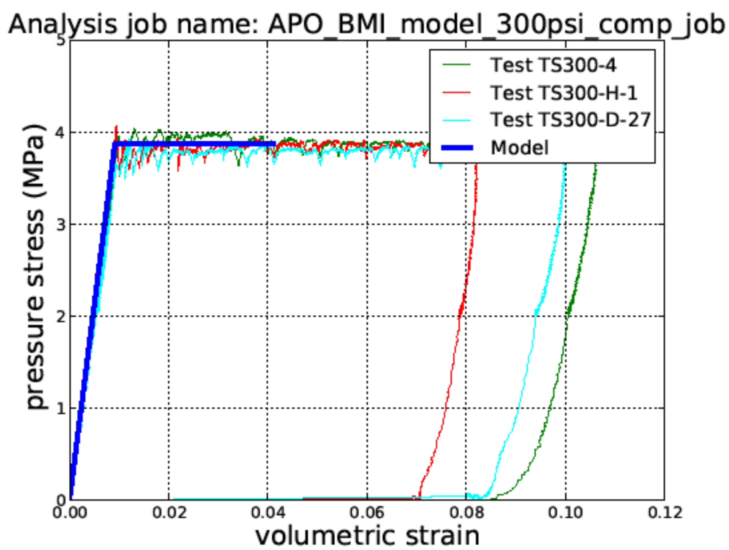

(b)

Figure B 6. Pressure stress versus volumetric strain during axial compression with 300psi of pressure for (a) the conservative and (b) the not-conservative models compared to all UNM tests at this condition.

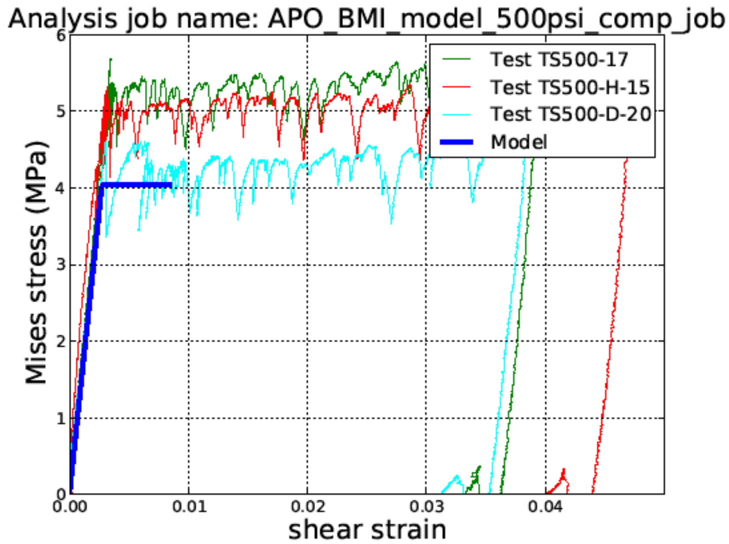

(a)

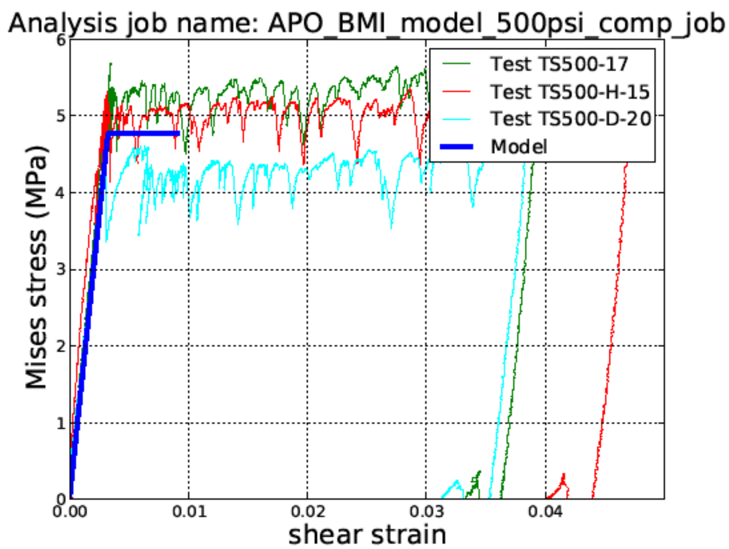

(b)

Figure B 7. Mises stress versus shear strain during axial compression with 500psi of pressure for (a) the conservative and (b) the not-conservative models compared to all UNM tests at this condition.

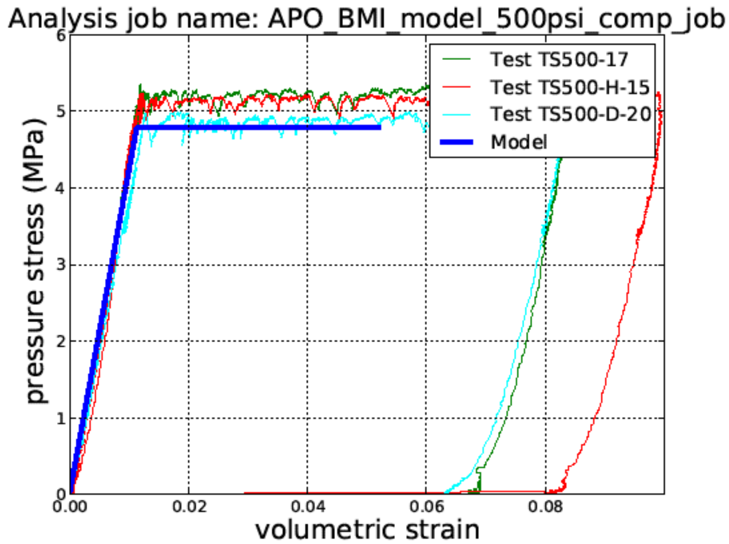

(a)

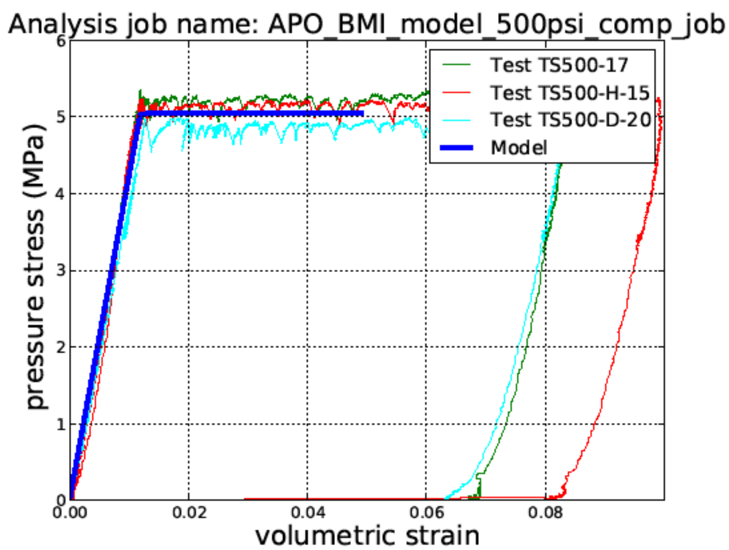

(b)

Figure B 8. Pressure stress versus volumetric strain during axial compression with 500psi of pressure for (a) the conservative and (b) the not-conservative models compared to all UNM tests at this condition.

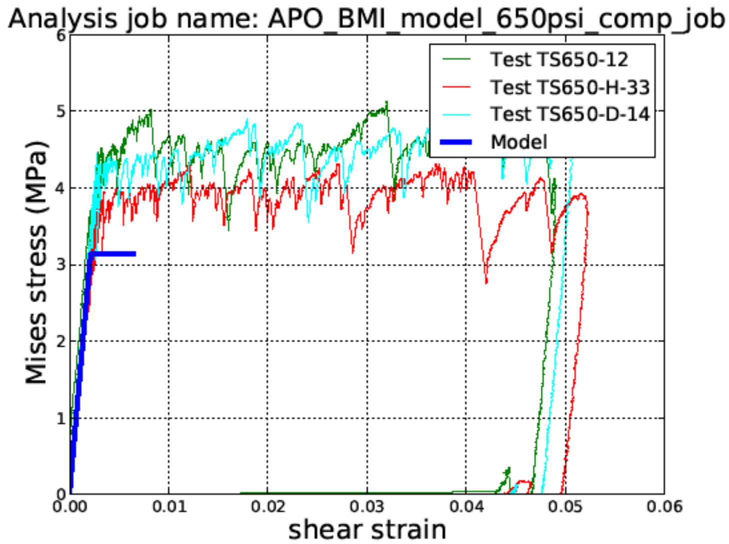

(a)

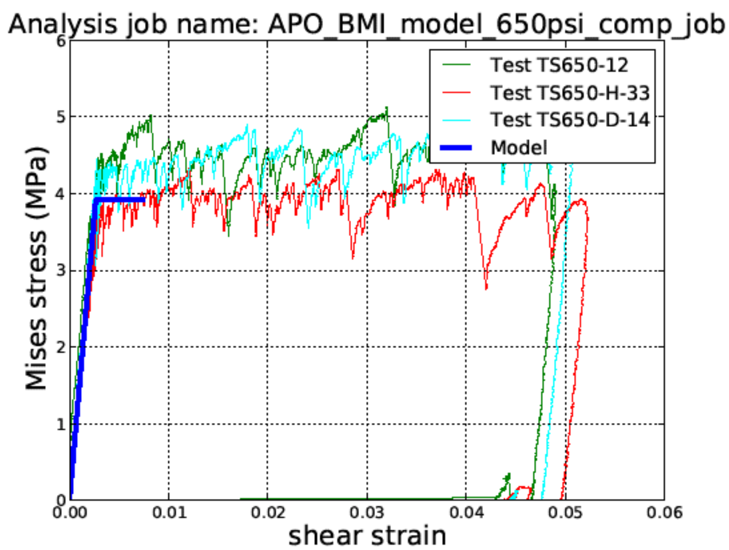

(b)

Figure B 9. Mises stress versus shear strain during axial compression with 650psi of pressure for (a) the conservative and (b) the not-conservative models compared to all UNM tests at this condition.

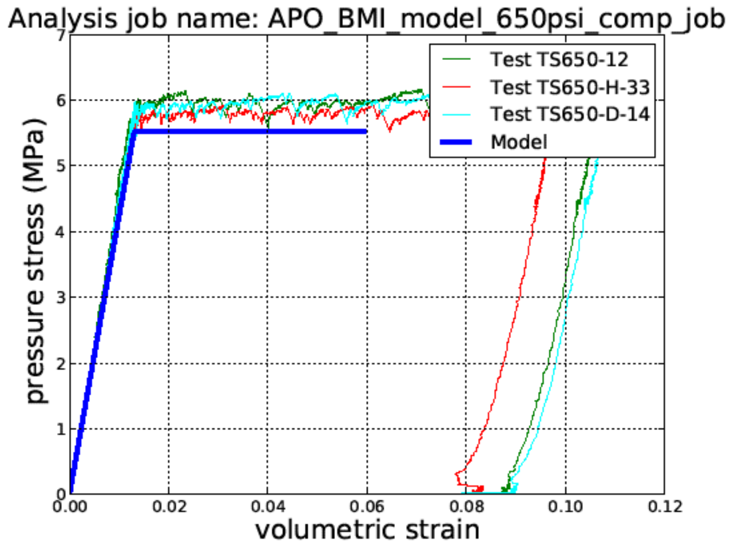

(a)

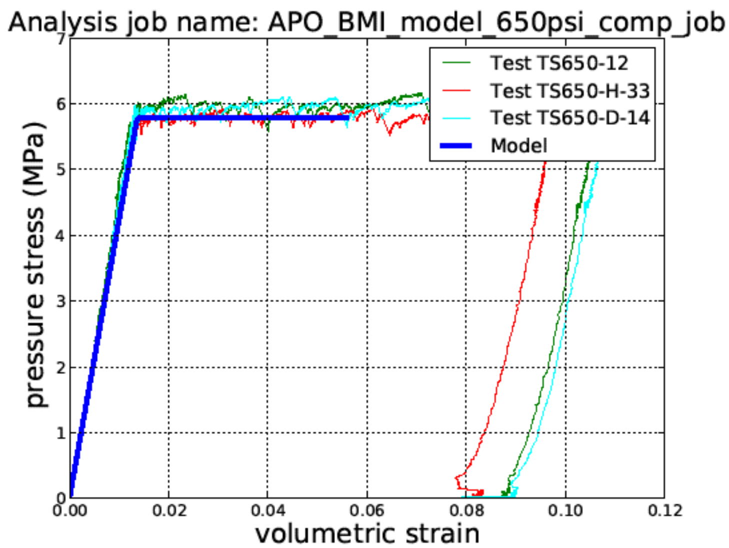

(b)

Figure B 10. Pressure stress versus volumetric strain during axial compression with 650psi of pressure for (a) the conservative and (b) the not-conservative models compared to all UNM tests at this condition.

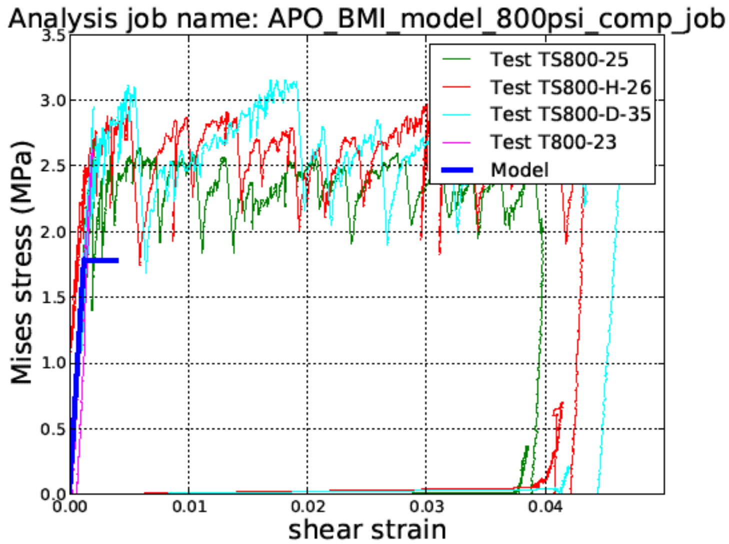

(a)

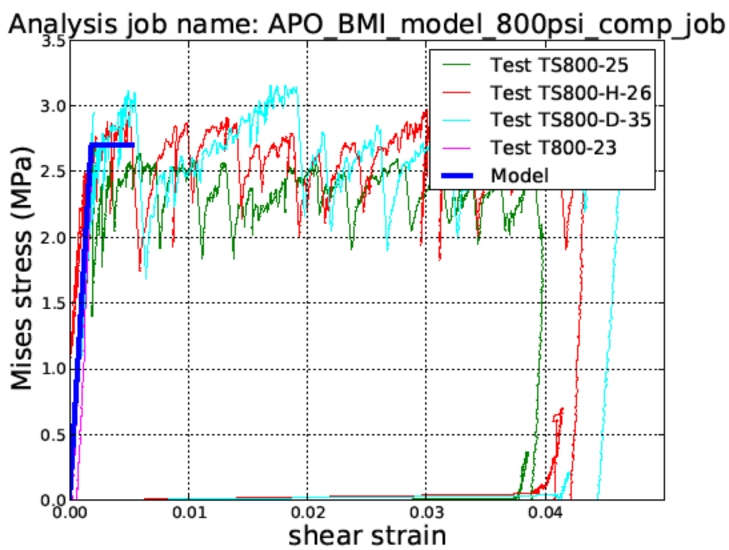

(b)

Figure B 11. Mises stress versus shear strain during axial compression with 800psi of pressure for (a) the conservative and (b) the not-conservative models compared to all UNM tests at this condition.

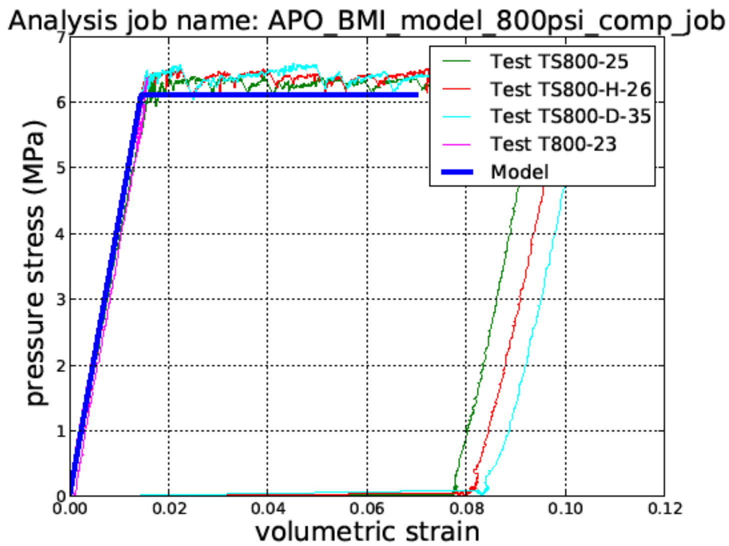

(a)

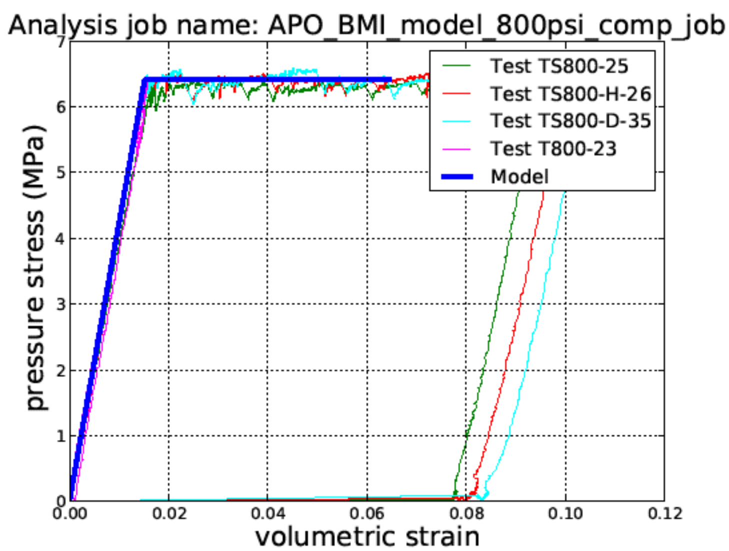

(b)

Figure B 12. Pressure stress versus volumetric strain during axial compression with 800psi of pressure for (a) the conservative and (b) the not-conservative models compared to all UNM tests at this condition.

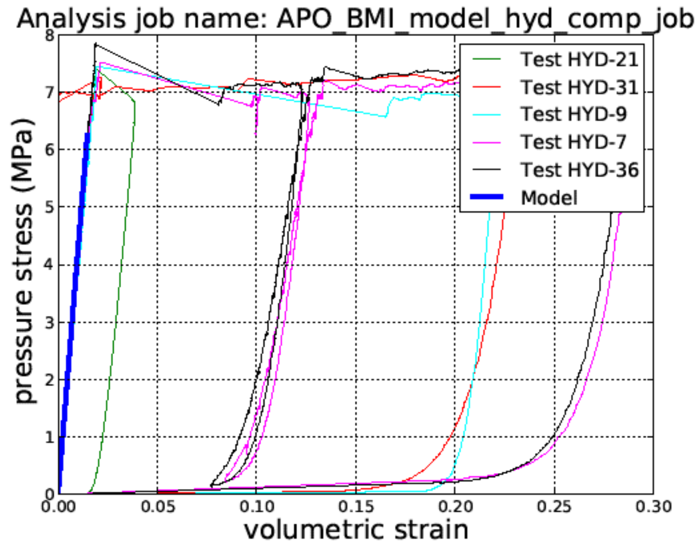

(a)

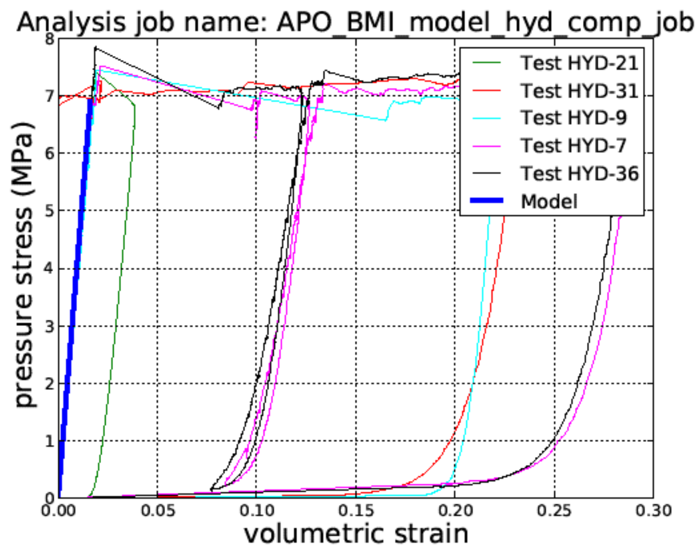

(b)

Figure B 13. Pressure stress versus volumetric strain under purely hydrostatic load for (a) the conservative and (b) the not-conservative models compared to all UNM tests at this condition.